Microporous and Mesoporous Materials 223 (2016) 196–202

Contents lists available at ScienceDirect

Microporous and Mesoporous Materials

journal homepage: www.elsevier.com/locate/micromeso

Structure and diffuse-boundary in hydrophobic and sodium dodecyl sulfate-modified silica aerogels

Amanda P. Perissinotto [a], Carlos M. Awano [a], Fabio S. de Vicente [a], Dario A. Donatti [a], Alexandre Mesquita [a], Luís F. da Silva [b], Dimas R. Vollet [a, *]

[a] Unesp – Univ Estadual Paulista, IGCE, Departamento de Física, Cx.P. 178, 13500-970 Rio Claro, SP, Brazil
[b] Unesp – Univ Estadual Paulista, IQ, Departamento de Bioquímica e Tecnologia, Rua Prof. Francisco Degni, 55, 14800-060 Araraquara, SP, Brazil

ARTICLE INFO

Article history:
Received 23 June 2015
Received in revised form
29 October 2015
Accepted 6 November 2015
Available online 18 November 2015

Keywords:
Diffuse-boundary
APD aerogels
Silylation
SAXS
Nitrogen adsorption

ABSTRACT

Small-angle X-ray scattering (SAXS) and nitrogen adsorption were used to study ambient pressure drying (APD) silica aerogels prepared from hydrolysis of tetraethoxysilane (TEOS) with additions of sodium dodecyl sulfate (SDS). The surfactant-extracted precursor wet gels have presented mass-fractal structure with typical fractal dimension 2.25 in a SAXS characteristic length scale from ~10 nm to ~0.35 nm. Hydrophobic APD aerogels with typical specific surface of 800 m^2/g and bulk density of 0.20 g/cm^3 were obtained after silylation of the precursor wet gels with a mixture of hexamethyldisiloxane (HMDSO) and trimethylchlorosilane (TMCS). The pore volume and the mean pore size of the APD aerogels increased with increasing the SDS quantity. APD aerogels presented most of the mass-fractal characteristics of the precursor wet gels at large length scales. The radius of gyration of the clusters of the APD aerogels (typically 17 nm) increased with increasing the SDS quantity, while the radius of the silica primary particles (typically 2.0 nm) increased at first with the addition of SDS (with respect to the sample without SDS) and decreased regularly afterward with increasing the SDS quantity. The primary particles presented yet some internal inhomogeneity and a diffuse-boundary interface with thickness of about 0.7 nm, according to a linear-gradient model for the diffuse boundary.

1. Introduction

Silica aerogels exhibit interesting structural properties often associated with low density and high specific surface [1], which make them be considered largely for scientific and technological applications in several areas of the knowledge as catalysis [2], adsorption [3], separation [4], sensing [5], thermal isolation [6], drug delivery [7], enzyme immobilization [8], and nanotechnology [9].

Drying is the most critical step in the obtaining of aerogels from the sol–gel process [10,11]. Conventional drying often causes collapse of the silica network due to capillary forces associated with the liquid surface tension. Supercritical extraction of the liquid phase of the wet gels (supercritical drying) often yields aerogels with structure not so far from that of the original wet gels, at least at large length scales. Supercritical drying (SCD) aerogels may be limited for application in some areas because they were hydrophilic (as they have OH end groups) and the structure of the aerogels could collapse even in moderate humid atmosphere with time [12,13]. Ambient pressure drying (APD), after a proper silylation pre-treatment on the silica surface, is an alternative method to prepare high-porosity hydrophobic aerogels [12–14], which diversifies the applicability of aerogels in several areas, since the hydrophobic surface of the APD aerogels prevents the structure deterioration in humid environments.

The process of obtaining hydrophobic APD aerogels requires a pre-treatment on the silica surface, named silylation, modifying the characteristic of the surface from hydrophilic to hydrophobic. Hexamethyldisiloxane (HMDSO) and trimethylchlorosilane (TMCS) are typical chemical silylating agents often used for this purpose [13]. Silylation replaces –H from hydrophilic Si–OH groups on the silica surface for stable hydrophobic $-SiR_3$ groups. Silylation also prevents the collapse of the silica network on drying provoked by capillary forces [11,13]. It would not be possible to dry the wet gel before the silylation if the aim is to obtain a sparse silica network as that of the aerogels, because of the collapsing of the silica network on drying occurring in the production of xerogels.

* Corresponding author. Tel.: +55 1935269179.
E-mail address: vollet@rc.unesp.br (D.R. Vollet).

http://dx.doi.org/10.1016/j.micromeso.2015.11.017
1387-1811/

Surfactants can form micelles and structural organization in a reactant silicate medium so they have been used as structure modifiers for a variety of mesoporous silica [15–18]. Particularly, sodium dodecyl sulfate (SDS) is an anionic surfactant which has been used in a few cases for this purpose [19–24]. In a previous work [23], a fixed quantity of SDS was used with varied quantities of an oil phase to produce hydrophobic APD silica aerogels. In a more recent work [24], we have obtained SCD aerogels in an autoclave, starting from a set of precursor wet gels prepared using varied quantities of SDS in the hydrolysis step of the process. It was concluded that the surface of the silica particles develops a surface-fractal characteristic with the supercritical process. In this work, the same set of precursor wet gels prepared with varied SDS quantities was used to produce hydrophobic APD aerogels, using a mixture of HMDSO and TMCS as silylating agent. The surface of the silica particles in the present APD aerogels showed completely different characteristics from that of the previous SCD aerogels, with the developing of a diffuse-boundary in the interface silica-pore, likely due to the attaching of hydrophobic groups on the silica surface. An original modified analytical approach was employed by incorporating the diffuse-boundary effect in the mass-fractal model characterizing the precursor wet gels, which was able to describe the SAXS curves in the whole q-domain (q being the modulus of the scattering vector), yielding complete characterization of the mass-fractal structure and the thickness of the diffuse-boundary of the present APD aerogels. The procedure certainly will be of interest for several researchers dealing with surface science. Interesting structural properties of the hydrophobic APD aerogels were yet inferred by combining small-angle X-ray scattering (SAXS) and nitrogen adsorption.

2. Material and methods

The APD aerogels were prepared from a set of silica wet gels prepared from acid hydrolysis of tetraethoxysilane (TEOS) in several water solutions of SDS. The water solutions of SDS were prepared with relative concentrations C_R (with respect to the SDS critical micelle concentration ~8.2×10^{-3} M) varying to $C_R = 0$, 1, 25, 50, 75 and 100. The hydrolysis of TEOS was carried out into the SDS solutions (after additions of ethanol and HCl) at 45 °C, so the TEOS/water/ethanol/HCl molar ratio was 1:26.5:0.78:0.070 while the SDS/TEOS molar ratio varied to 0, 0.0035, 0.0875, 0.175, 0.26 and 0.35. The hydrolyzed solutions were kept in sealed containers at 40 °C for gelation (which occurred in a few hours) and aging (for 5 days) to obtain monolithic wet gels. The wet gels were yet washed with water, ethanol, and *n*-hexane to remove the surfactant, non-reacted residues, and byproducts of hydrolysis.

APD aerogels were prepared after silylation of the wet gels by immersion in a solution of HMDSO and TMCS (the silylating agents) in isopropyl alcohol (IPA) and *n*-hexane as a solvent mixture [13]. The HMDSO/TMCS/IPA/*n*-hexane molar ratio of the silylating solution was 1:1:1:1. The silylation was carried out under mechanical stirring at ambient temperature for 5 days, being the silylating solution renewed at each 24 h. The excess of the silylation agents was removed by washing in *n*-hexane. The silylated gels were allowed to dry under ambient pressure for 3 days at 40 °C to obtain hydrophobic APD aerogels samples. The APD aerogels were yet degassed at 120 °C in vacuum conditions (~3×10^{-3} mmHg) for about 24 h before they were studied by nitrogen adsorption and SAXS.

The SAXS experiments were carried out using synchrotron radiation with a wavelength $\lambda = 0.1608$ nm at the SAXS beamline of the National Synchrotron Light Laboratory (LNLS), Campinas, Brazil, using a pinhole geometry for the X-ray beam collimation. A 2D position sensitive X-ray detector was used to obtain high precision data for the isotropic SAXS intensity $I(q)$ as a function of the modulus of the scattering vector $q = (4\pi/\lambda)\sin(\theta/2)$, where θ is the scattering angle. The experimental SAXS data were measured from $q_0 = 0.1379$ nm^{-1} up to $q_m = 3.3480$ nm^{-1} with resolution of about 4×10^{-4} nm^{-1}. The data were corrected by sample attenuation and parasitic scattering (the scattering produced without the sample) and normalized with respect to the beam intensity. No additional background subtraction was carried out in the corrected and normalized SAXS data, neither for the present APD aerogels nor for the original wet gels studied earlier. The scattering intensity data were analyzed as obtained in relative units, without normalization to any standard to have absolute units.

Nitrogen adsorption isotherms were obtained at liquid nitrogen temperature (77 K) by using an ASAP 2010 Micromeritics apparatus. The data were analyzed for the BET specific surface, the total pore volume (as the nitrogen adsorbed volume at a point close to the nitrogen saturation pressure, $p/p_0 \sim 0.984$), and the mean pore size.

3. Results and discussion

3.1. SAXS

Fig. 1 shows the curves of the SAXS intensity $I(q)$ for the hydrophobic APD aerogels in direct comparison with those of the original precursor wet gels. A little-modified but basically the same

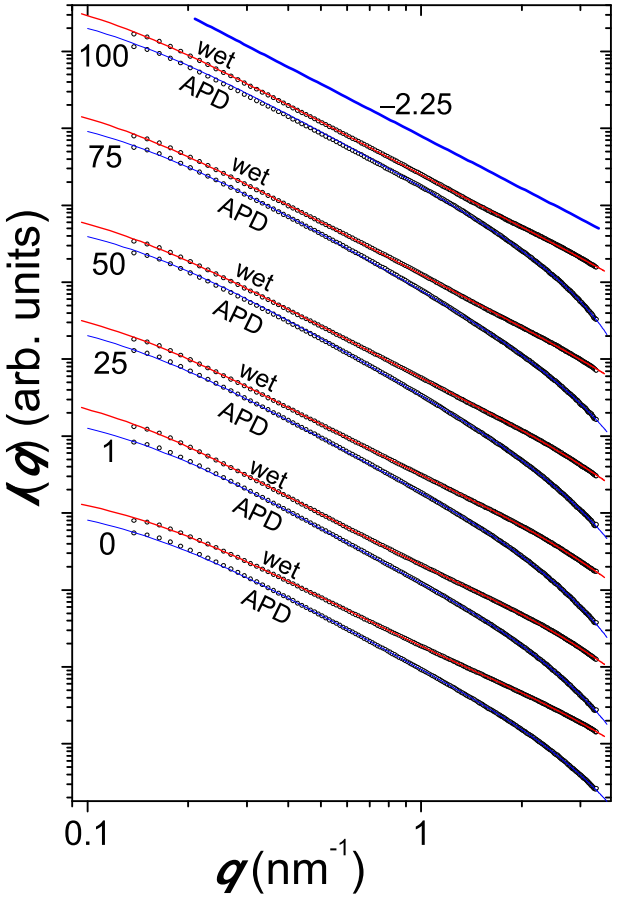

Fig. 1. SAXS patterns for the APD aerogels compared to those of the precursor wet gels. Numbers represent the SDS relative concentration C_R used in the preparation of the gels. The curves were vertically shifted for the sake of clarity. The full lines were drawn from fitting processes of the models (see the text) to the experimental data (points). A straight line with slope equal to −2.25 was drawn as a reference.

model used in the SAXS structural characterization of the precursor wet gels [24] was used here to study the present APD aerogels.

The structure of the precursor wet gels was described in terms of a mass-fractal system for which the SAXS intensity could be decomposed as [25,26].

$$I(q) = AP(q)S(q), \tag{1}$$

where A is a constant, $S(q)$ is the structure factor of the mass-fractal cluster, and $P(q)$ is the form factor of an individual scatter. $S(q)$ was approached by Ref. [25].

$$S(q) = 1 + B\Gamma(D+1)\sin[(D-1)\arctan(q\xi)] \Big/ \left(1+q^2\xi^2\right)^{(D-1)/2}(D-1)q\xi, \tag{2}$$

where $B = (\xi/r_a)^D$ (r_a being the gauge of measurement of the characteristic primary particle size) represents the number of primary particles in a cluster of characteristic size ξ and fractal dimension D, and $\Gamma(D+1)$ is the gamma function of the argument $(D+1)$. $P(q)$ was approximated by the Debye–Bueche form [27,28].

$$P(q) = 1/\left(1+a_0^2q^2\right)^2, \tag{3}$$

where a_0 is a correlation distance associated with the structure of the primary particle. Equation (1) is dominated by the factor $S(q)$ at low- and intermediary-q for systems with a_0 small enough. Under this conditions, the second term of $S(q)$ in eq (2) is too much larger than 1, exhibiting a Guinier's law behavior at low-q and crossing over at $q \sim \xi^{-1}$ to a power-law on q as $S(q) \propto q^{-D}$. In the Porod law region ($q \to \infty$), the second term of $S(q)$ in eq (2) is too smaller than 1 and eq (1) is dominated by $P(q)$. These characteristics were found in the SAXS curves from the original wet gels in Fig. 1. The parameters ξ, D, a_0, and B were obtained by fitting eq (1) with eqs (2) and (3) to the experimental data of the wet gels [24]. These results were included in Table 1 of the present work in order to directly compare them with those from the present APD aerogels.

Fig. 1 shows the modifications in the SAXS curves provoked by the overall silylation and ambient pressure drying (APD) process in the obtaining of APD aerogels. The SAXS curves of the APD aerogels presented the same characteristics as those of the precursor wet gels at low- and intermediary-q, since the corresponding curves were found practically parallel at low- and intermediary-q, and exhibited a very pronounced crossover at high-q, a rather shifted to the intermediary-q side when compared to the wet gels. The picture suggests that most of the large-scale mass-fractal structure of the original wet gels (associated to the contribution at low- and intermediary-q) was kept under the overall silylation and APD process, even though only in a limited range of the length scale (the large-scale structure) for which perhaps the auto-similarity that the fractality requires could not be completely met. However, the description of power-law objects as fractal is yet justified and useful as it provides a simple model to describe ill-defined geometries, even though it does not imply fractality at all [29]. The shifting of the high-q crossover towards the intermediary-q region means that the primary particles (associated to the cutoff distances a_0) building up the fractal cluster are larger in the APD aerogels in comparison with those in the precursor wet gels.

A more meticulous exam of the decaying of $I(q)$ at high-q of the APD aerogels in Fig. 1 shows that $I(q)$ decays more rapidly than the Porod law $I(q) \propto q^{-4}$, which means a negative departure from Porod's law. The negative departure from Porod's law is better seen in a $I(q)q^4$ *vs* q plot, as shown in Fig. 2 for the APD aerogels, where the quantity $I(q)q^4$ was found diminishing continuously at high-q, instead to be a constant as in Porod's law.

Negative departure from Porod's law has been attributed to the presence of a diffuse-boundary at the interface of a two-phase system [30]. We attributed the presence of the diffuse-boundary in the APD aerogels to the attaching of hydrophobic organic groups on the silica surface, forming a layer composed by many $-O-Si\equiv(CH_3)_3$ groups giving rise to an electron-density gradient across the silica-pore interface. Koberstein et al. [30] have pointed that a linear electron-density gradient across the interface with diffuse-boundary thickness E yields an observable SAXS intensity in the Porod region given by

$$\lim_{q\to\infty} I(q) = \left(K_p/q^4\right)\left(1 - E^2q^2/12\right), \tag{4}$$

where $K_p = \lim_{q\to\infty} I(q)q^4$ is the Porod law constant in the absence of the diffuse boundary. The model described by eq (1) with eqs (2) and (3) in the present work yields $\lim_{q\to\infty} I(q)q^4 = (A/a_0^4)$, meaning that $K_p = (A/a_0^4)$ in the absence of the diffuse boundary. Then it is licit to rewrite $P(q)$ as

$$P(q) = \left[1/\left(1+a_0^2q^2\right)^2\right]\left(1 - E^2q^2/12\right) \tag{5}$$

in presence of the diffuse-boundary to use the same model to describe both the wet gels and the APD aerogels. Naturally $\lim_{q\to\infty} I(q)$ using eq (1) with $P(q)$ given by eq (5) yields eq (4) with $K_p = (A/a_0^4)$, since $\lim_{q\to\infty} S(q) = 1$.

The SAXS curves of the APD aerogels were then fitted by eq (1) with the same structure factor $S(q)$ given by eq (2) but with $P(q)$ given by eq (5). For the fitting process, the parameters ξ and D were firstly obtained from fitting the structure factor $S(q)$ (eq (2)) at low- and intermediary-q portion of the SAXS curve, then other parameters (A, B, a_0, and E) were fitted by eq (1) with eqs (2) and (5) to the whole experimental $I(q)$ curve using a $I(q)q^4$ *vs* q plot, as shown in Fig. 2. The fitted parameters ξ, D, B, a_0, and E are shown in Table 1 for the APD aerogels.

Table 1
SAXS parameters of the precursor wet gels and APD aerogels.

C_R	ξ (nm)		D		a_0 (nm)		B (10^2)		E (nm)
	Wet[a]	APD	Wet[a]	APD	Wet[a]	APD	Wet[a]	APD	APD
0	8.17 (8)	7.70 (7)	2.22 (1)	2.29 (1)	0.32 (1)	0.49 (1)	1.7 (1)	1.1 (1)	0.63 (3)
1	9.64 (9)	8.21 (8)	2.32 (1)	2.33 (1)	0.43 (1)	0.60 (1)	1.8 (1)	0.8 (1)	0.68 (3)
25	9.78 (9)	8.98 (8)	2.27 (1)	2.30 (1)	0.44 (1)	0.60 (1)	1.7 (1)	1.0 (1)	0.70 (3)
50	10.3 (1)	8.46 (8)	2.24 (1)	2.32 (1)	0.38 (1)	0.57 (1)	3.1 (2)	1.3 (1)	0.67 (3)
75	11.0 (1)	9.23 (9)	2.23 (1)	2.28 (1)	0.27 (2)	0.50 (1)	8.7 (9)	2.2 (2)	0.67 (3)
100	11.3 (1)	10.1 (1)	2.26 (1)	2.25 (1)	0.23 (3)	0.48 (1)	12 (1)	2.4 (2)	0.76 (3)

[a] From ref. [24].

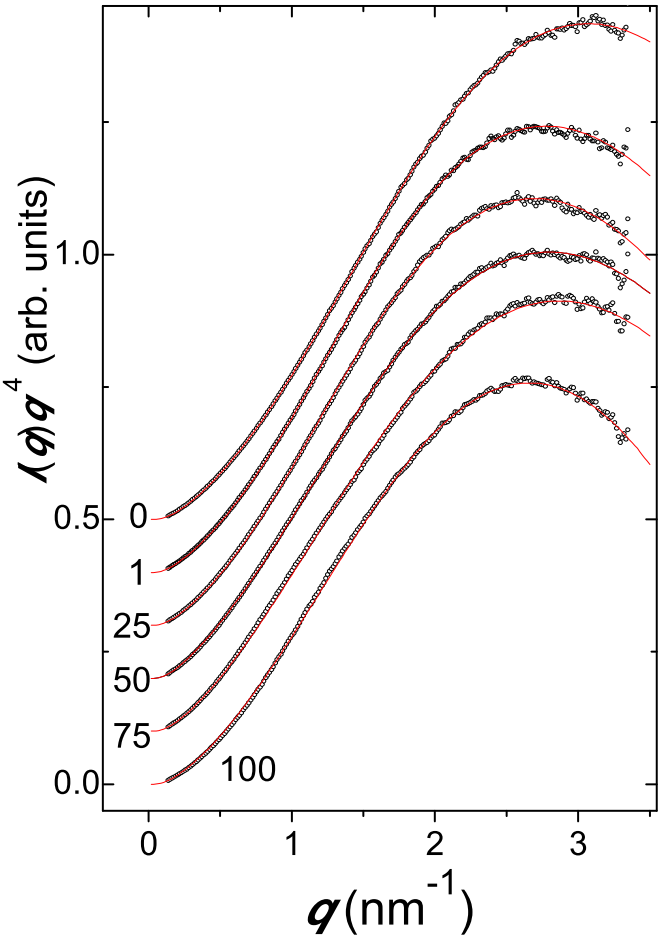

Fig. 2. Typical Porod's law plots for the APD aerogels suggesting an interface with diffuse-boundary. Numbers represent the SDS relative concentration C_R used in the preparation of the gels. The curves were conveniently shifted for the sake of clarity. The full lines were fittings of the eq (1), through eqs (2) and (5), to the experimental data (points).

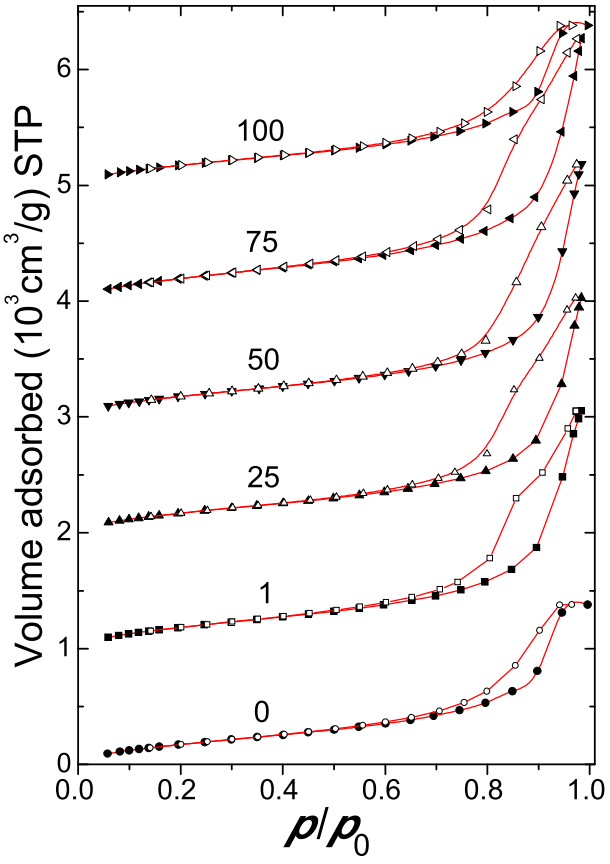

Fig. 3. Nitrogen adsorption isotherms for the APD aerogels. Open symbols correspond to the desorption branch. Numbers represent the SDS relative concentration C_R used in the preparation of the gels. Isotherms were shifted 1000 cm^3/g with respect to the others for the sake of clarity.

The characteristic size ξ of the fractal cluster in the APD aerogels diminished only about 10% with respect to the original wet gels, while the fractal dimension D increased slightly as a result of the overall silylation and APD process. The number of primary particles per cluster B diminished significantly with the APD process with respect to the original wet gels, because of the modification and growing of the primary particles building up the fractal clusters. The typical value found for the diffuse-boundary thickness was $E \sim 0.7$ nm (Table 1), a rather larger than that expected from a single layer formed by hydrophobic $-O-Si\equiv(CH_3)_3$ groups on the silica surface. This suggests that the diffuse boundary could be a more complex structure formed by silica species and hydrophobic organic groups on the silica surface as a result of the overall silylation and APD process. The diffuse-boundary has not been observed earlier in the analogous system studied previously [23] because the maximum q_m probed by SAXS there was 2.34 nm^{-1}, which is below the high-q range showing the effect of the diffuse-boundary in Fig. 2.

3.2. Nitrogen adsorption

Fig. 3 shows the nitrogen adsorption isotherms of type IV obtained for the APD aerogels. Table 2 shows the specific surface area S_{BET}, the specific pore volume V_p and the mean pore size $l_p = 4V_p/S_{BET}$ obtained from the isotherms.

S_{BET} of the APD aerogels was typically 800 m^2/g (without strong dependency on the SDS quantity), while the pore volume V_p and the mean pore size l_p were found larger in the APD aerogels prepared with SDS (when compared to that without SDS) and increasing slightly with increasing the SDS quantity (Table 2). The increase of V_p is compatible with the increase of characteristic size ξ of the fractal cluster as observed by SAXS (Table 1), because as larger is the quantity of SDS micelles, larger are the spaces filled by the surfactant during the earlier gelation process, increasing the pore volume and the fractal cluster size. The apparent discrepancy in V_p found in the sample with $C_R = 100$ (V_p was unexpectedly found smaller in this sample with respect to other samples prepared with SDS) could be explained because conventional nitrogen adsorption can underestimate the pore volume in a sparse silica network, since the adsorbate/vapor interface can adopt a surface of zero curvature while much of the larger pores remains empty [31,32]. The extent of the phenomenon is larger as larger the pore/particle size ratio,

Table 2
Structural properties of the APD aerogels as determined from nitrogen adsorption.

C_R	S_{BET} (m^2/g)	V_p (cm^3/g)	l_p (nm)
0	859 (7)	2.41 (1)	11.2 (2)
1	794 (7)	3.07 (1)	15.4 (2)
25	744 (6)	3.01 (1)	16.2 (2)
50	771 (6)	3.27 (1)	16.8 (2)
75	844 (7)	3.34 (1)	15.8 (2)
100	737 (6)	2.13 (1)	11.6 (2)

which was expected to be the largest one for the sample with $C_R = 100$. This effect was also observed in the SCD aerogel produced from the same precursor wet gel with $C_R = 100$ [24].

3.3. SAXS and nitrogen adsorption correlation data

The meaning of the parameters used in the present model to describe the structure of APD aerogels should be better specified in each case. The radius of gyration R_g of a mass-fractal cluster with fractal dimension D is related to the characteristic size ξ by Ref. [26] $R_g = [D\,(D+1)/2]^{1/2}\xi$. The parameter a_0 in the Debye–Bueche form (eq (3)) was originally assigned to an inhomogeneity correlation distance in a random disordered material [27], for which the correlation function is $\gamma(r) = \exp(-r/a_0)$. In the case of $P(q)$ could be approximated by the scattering from a so small primary particle at high-q through a Guinier's law of the type $P(q) \cong (1-2a_0^2q^2)$, the radius r_0' of an equivalent spherical particle would be given by $r_0' = 10^{1/2}a_0$. The parameter $B = (\xi/r_a)^D$ gives the number of primary particles per cluster with characteristic size r_a as measured by the same gauge of measurement used for the characteristic size ξ of the cluster. More fundamentally, the number of primary particles per cluster is written in terms of the radius of gyration of the cluster [33,34] as $B = (R_g/r_0)^D$, where r_0 is the true radius of primary particle as measured by the same gauge of measurement used for R_g. We think r_0 and r_0' should represent the same parameter, however in a_0 could there be some contribution of Porod's law type due to some internal inhomogeneity in the primary particles (as it will be shown), which would diminish the measured a_0 making r_0' apparently smaller than r_0.

Table 3 shows the SAXS parameters R_g, r_0', r_0 and $r_0 + E$ evaluated for the APD aerogels. R_g was evaluated using $R_g = [D\,(D+1)/2]^{1/2}\xi$ with the experimental ξ and D in Table 1. The radius r_0' was evaluated as $r_0' = 10^{1/2}a_0$ from a_0 in Table 1. The primary particle radius r_0 was evaluated using R_g from Table 3 and the experimental B and D in Table 1 as

$$r_0 = R_g \Big/ B^{1/D}. \tag{6}$$

The radius of gyration R_g of the APD aerogels (typically 17 nm) increased (accompanying the characteristic size ξ) with increasing the SDS quantity. The radius r_0' (typically 1.7 nm) of the primary particles, as evaluated from the Guinier approximation for $P(q)$, was found somewhat smaller than the radius r_0 (typically 2.0 nm), as evaluated from the number of particles per cluster B, which suggests some internal inhomogeneity in the primary particles. The radius r_0 of the primary particles of the aerogels increased at first with the addition of SDS (with respect to the sample without SDS) and decreased afterward with increasing the SDS quantity. This result is in agreement with that just inverse behavior found for the number of primary particle per cluster B (Table 1) for the APD aerogels.

The specific surface S_{BET} of the APD aerogels is expected to match with that of a spherical primary particle with density ρ_s and radius r_0+E (Table 3), because of the thickness E of the diffuse-boundary interface, or $S_{BET} = 3/(r_0 + E)\rho_s$. The evaluation of $S_{BET} = 3/(r_0+E)\rho_s$ with the experimental $r_0 + E$ (from SAXS) in Table 3, using 2.2 g/cm^3 (the density of the fused silica) for ρ_s, yields values for S_{BET} which are about 35% smaller than that experimental ones in Table 2. This apparent disagreement in the evaluated S_{BET} corroborates the hypothesis of some structural inhomogeneity in the primary particles in the APD aerogels, as suggested by the finding $r_0' < r_0$, which makes the particle density ρ_s smaller than that of the fused silica. Internal structural inhomogeneity was also found in the primary particles of the earlier SCD aerogels [24] obtained from the same set of SDS-modified precursor wet gels used in the present work. This suggests all these common low-temperature sol–gel processes yield not too compact silica particles when compared to fused silica.

Thus the primary particle density ρ_s was evaluated as $\rho_s = 3/S_{BET}(r_0 + E)$ in order to match with both the experimental S_{BET} (from nitrogen adsorption) and $r_0 + E$ (from SAXS). The values found for ρ_s shown in Table 4 are signifying smaller than the density of the fused silica. Table 4 shows that ρ_s decreased at first with the addition of SDS (with respect to the sample without SDS) and increased regularly afterward with increasing the SDS quantity, just in agreement with the inverse behavior found for the radius r_0 of the primary particle (Table 3). The skeletal density ρ_{IPA} was directly measured with a 5-cm^3 glass pycnometer using IPA as the filling liquid (because IPA is solvent of the silylating agents and would be able to penetrate the mesopores) and the results were found in good agreement with the evaluated ρ_s from SAXS and nitrogen adsorption (Table 4). This finding suggests good correlation between the parameters inferred from SAXS and nitrogen adsorption in describing the structural characteristics of the primary particles in the APD aerogels, mainly with respect to their size ($r_0 \sim 2.0$ nm), diffuse boundary ($E \sim 0.7$ nm) and internal inhomogeneity ($\rho_s \sim \rho_{IPA} \sim 1.4$ g/cm^3). Particularly, the diffuse boundary has been assigned to the negative departure from Porod'law at high-q approximately in the range $q_L < q < q_m$, being the inferior limit q_L typically ~2.5 nm^{-1} (Fig. 2) and $q_m \sim 3.5$ nm^{-1} (the maximum experimental accessed q). Kalliat et al. [35] have established that Porod's law is quite well satisfied when $qD_{min} \geq 3.5$, where D_{min} is the smallest dimension of the scattering particle. The typical particle size $r_0 \sim 2.0$ nm inferred from either SAXS (eq (6)) or nitrogen adsorption (from $r_0 + E = 3/S_{BET}\rho_s$) in the present work (see also Fig. S1 showing clusters formed by primary particles with radius r_0 typically between 2 and 4 nm) is compatible with the fulfilling of the condition $qr_0 \geq 3.5$ in the range $q_L < q < q_m$ used to probe the diffuse boundary. The Debye–Bueche factor (eq (6)) employed to describe de primary particle scattering in the present system does not give a sharp crossover to a Porod's law at high-q, but it surely does not give a maximum in a $I(q)q^4$ *vs* q Porod plot like that in Fig. 2. We thought the Debye–Bueche form could be accounting for share of the contributions of the internal inhomogeneity of the primary particles responsible for the relative low density of the primary particles ($\rho_s \sim \rho_{IPA} \sim 1.4$ g/cm^3).

The robustness of the present model applied to the APD aerogels was also probed by determining the bulk density as measured by

Table 3
Structural properties of the APD aerogels as evaluated from SAXS.

C_R	R_g (nm)	r_0' (nm)	r_0 (nm)	r_0+E (nm)
0	14.9 (3)	1.55 (3)	1.90 (5)	2.5 (1)
1	16.2 (3)	1.89 (4)	2.44 (5)	3.1 (1)
25	17.5 (3)	1.91 (4)	2.36 (5)	3.1 (1)
50	16.6 (3)	1.80 (4)	2.05 (5)	2.7 (1)
75	17.8 (3)	1.58 (3)	1.68 (4)	2.3 (1)
100	19.3 (4)	1.52 (3)	1.69 (4)	2.5 (1)

Table 4
Skeletal and bulk densities as measured experimentally or evaluated from SAXS and nitrogen adsorption.

C_R	ρ_s (g/cm^3)	ρ_{IPA} (g/cm^3)	ρ_ξ (g/cm^3)	ρ_{N2} (g/cm^3)	ρ_{gly} (g/cm^3)
0	1.4 (1)	1.3 (1)	0.32 (3)	0.32 (2)	0.20 (1)
1	1.2 (1)	1.1 (1)	0.34 (3)	0.26 (2)	0.22 (1)
25	1.3 (1)	1.4 (1)	0.32 (3)	0.27 (2)	0.19 (1)
50	1.4 (1)	1.5 (1)	0.34 (3)	0.25 (2)	0.17 (1)
75	1.5 (1)	1.6 (1)	0.28 (2)	0.25 (2)	0.18 (1)
100	1.7 (1)	1.5 (1)	0.27 (2)	0.37 (2)	0.19 (1)

different methods. The bulk density ρ_{N2} as measured from nitrogen adsorption was evaluated by using the equation $(1/\rho_{N2}) = (1/\rho_s) + V_p$, with the experimental V_p in Table 2 (from nitrogen adsorption) and ρ_s from Table 4. The bulk density ρ_ξ as measured from SAXS can be cast as [36] $\rho_\xi = \rho_s (R_g/r_0)^{D-3}$ and, since $B = (R_g/r_0)^D$, ρ_ξ was evaluated as

$$\rho_\xi = \rho_s B^{(D-3)/D} \tag{7}$$

with the experimental B and D in Table 1 (from SAXS) and ρ_s from Table 4. The bulk density ρ_{gly} of the APD aerogels was also measured by a 5-cm^3 glass pycnometer using glycerin as the filling liquid, since glycerin (like water) could not penetrate the mesopore structure because the hydrophobic characteristic of the APD aerogels. Table 4 shows the evaluated ρ_ξ and ρ_{N2} and the measured ρ_{gly}.

The value of ρ_ξ was found in agreement with ρ_{N2} in the case of the APD aerogel prepared without SDS (Table 4). With the additions of SDS, ρ_ξ was found diminishing with increasing the SDS quantity, while ρ_{N2} was found on the average about 12% smaller than ρ_ξ but diminishing only very slightly with increasing the SDS quantity, except for the sample with $C_R = 100$ for which ρ_{N2} was found abnormally high, because the abnormally small V_p found for this sample (Table 2), as discussed earlier. The reasonable agreement between the values between ρ_ξ and ρ_{N2} suggests that most of the mesoporosity recorded by nitrogen condensation could be assigned to the mesoporosity permeating the fractal cluster seen by SAXS. The lower rate of diminution of ρ_{N2} compared to ρ_ξ with increasing the SDS quantity (and the abnormal high value found for ρ_{N2} in the sample with $C_R = 100$) could be explained because the underestimating of the pore volume by nitrogen condensation in sparse silica networks [31,32], as mentioned earlier, is larger as larger the pore/particle size ratio, which was expected to be larger in APD aerogels prepared with higher SDS quantities, particularly for the sample with $C_R = 100$. The bulk densities ρ_{gly} were found not too dependent on the SDS quantity, presenting a typical value of about 0.20 g/cm^3 (Table 4), which is about 30% smaller than the typical values found for ρ_ξ and ρ_{N2}. This result suggests that about 10% of the total porosity $\phi = 0.86$ found on the average in the APD aerogels (as evaluated by $\phi = (\rho_s - \rho_{gly})/\rho_s$) could be composed by macropores (or large mesopores) outside of the fractal clusters, neither accounted by SAXS nor nitrogen condensation.

Fig. 4 resumes in a sketched way the structural characteristics of the present APD aerogels which could be inferred from the present model based on SAXS and nitrogen adsorption. The structural characteristics sketched in Fig. 4 are in reasonable agreement with those inferred from the TEM image of Fig. S1, obtained for a typical APD aerogel, where is apparent an agglomeration of clusters of about 50 nm diameter formed by primary particles with radius typically between 2 and 4 nm.

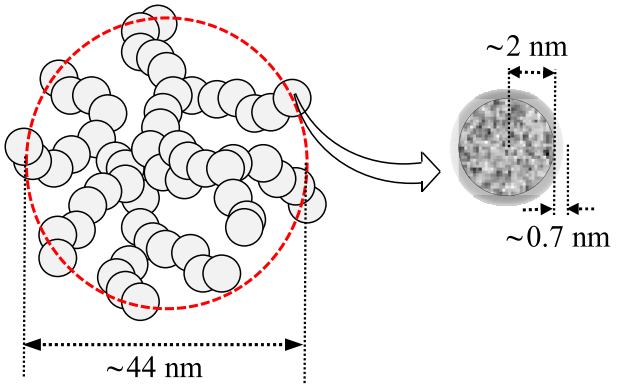

Fig. 4. A sketch of the structure of the APD aerogels as inferred from SAXS and nitrogen adsorption, showing a cluster with radius of gyration R_g ~ 17 nm represented by an equivalent sphere with diameter of ~44 nm.

4. Conclusions

Hydrophobic APD silica aerogels, with typical specific surface of 800 m^2/g and bulk density of 0.20 g/cm^3, were obtained after silylation (with a mixture of HMDSO and TMCS) from a set of wet gels prepared from TEOS hydrolysis with additions of SDS. The surfactant-extracted precursor wet gels presented a mass-fractal structure with typical fractal dimension 2.25 in a SAXS characteristic length scale from ~10 nm to ~0.35 nm.

The pore volume and the mean pore size of the APD aerogels increased with increasing the SDS quantity. The APD aerogels presented most of the mass-fractal characteristics of the precursor wet gels at large length scales. The radius of gyration of the fractal clusters of the APD aerogels (typically 17 nm) increased with increasing the SDS quantity. The radius of the primary particles (typically 2.0 nm) building up the fractal cluster increased at first with the addition of SDS (with respect to the sample without SDS) and decreased afterward with increasing the SDS quantity.

The silica primary particles in the APD aerogels presented yet some internal inhomogeneity and a diffuse-boundary interface with thickness E ~ 0.7 nm, according to a linear-gradient model for the diffuse boundary. The diffuse-boundary is likely formed by a complex structure involving silica species and hydrophobic organic groups on the silica surface as a result of the overall silylation and APD process.

Acknowledgment

This work was supported by the Brazilian Synchrotron Light Laboratory (LNLS), FAPESP, and CNPq, Brazil.

Appendix A. Supplementary data

Supplementary data related to this article can be found at http://dx.doi.org/10.1016/j.micromeso.2015.11.017.

References

[1] C.J. Brinker, G.W. Scherer, Sol-gel Science: the Physics and Chemistry of Sol-gel Processing, Academic Press, New York, 1990.
[2] G.M. Pajonk, Aerogel catalysts, Appl. Catal. 72 (1991) 217–266.
[3] L.W. Hrubesh, P.R. Coronado, J.H. Satcher Jr., J. Non-Cryst. Solids 285 (2001) 328–332.
[4] S. Štandeker, Z. Novak, Ž. Knez, J. Colloid Interface Sci. 310 (2007) 362–368.
[5] M.K. Carroll, A.M. Anderson, Aerogels as platforms for chemical sensors, in: M. Aegerter, N. Leventis, M.M. Koebel (Eds.), Aerogels Handbook, Springer, New York, 2011, p. 637.
[6] K. Kamiuto, T. Miyamoto, S. Saitoh, Appl. Energ 62 (1999) 113–123.
[7] I. Smirnova, S. Suttiruengwong, W. Arlt, J. Non Cryst. Solids 350 (2004) 54–60.
[8] N. Kharrata, Y. Ben Ali, S. Marzoukb, Y.-T. Gargouria, M. Karra-Chaabounia, Process Biochem. 46 (2011) 1083–1089.
[9] N. Gaponik, A. Wolf, R. Marx, V. Lesnyak, K. Schilling, A. Eychmüller, Adv. Mater 20 (2008) 4257–4262.
[10] G.W. Scherer, J. Non Cryst. Solids 100 (1988) 77–92.
[11] G.W. Scherer, J. Non Cryst. Solids 147–148 (1992) 363–374.
[12] P.B. Sarawade, J.K. Kim, H.K. Kim, H.T. Kim, Appl. Surf. Sci. 254 (2007) 574–579.
[13] A. Parvathy Rao, A. Venkateswara Rao, J. Mater. Sci. 45 (2010) 51–63.
[14] A.M. Anderson, M.K. Carroll, Hydrophobic silica aerogels: review of synthesis, properties and applications, in: M. Aegerter, N. Leventis, M.M. Koebel (Eds.), Aerogels Handbook, Springer, New York, 2011, p. 47.
[15] E. Prouzet, T.J. Pinnavaia, Angew. Chem. Int. Ed. 36 (1997) 516–518.
[16] S.A. Bagshaw, E. Prouzet, T.J. Pinnavaia, Templating of mesoporous molecular sieves by nonionic polyethylene oxide surfactants, Science 269 (1995) 1242–1244.
[17] K. Aikawa, K. Kaneko, T. Tamura, M. Fujitsu, K. Ohbu, Colloids Surf. A 150 (1999) 95–104.

[18] D. Zhao, J. Feng, Q. Huo, N. Melosh, G.H. Fredrickson, B.F. Chmelka, G.D. Stucky, Science 279 (1998) 548–552.
[19] Q. Huo, D.I. Margolese, U. Cielta, D.G. Demuth, P. Feng, T.E. Gier, P. Sieger, A. Jirouzi, B.F. Chmelka, F. Schuth, G.D. Stucky, Chem. Mater 6 (1994) 1176–1191.
[20] Y.G. Lee, C. Oh, S.K. Yoo, S.M. Koo, S.G. Oh, Microporous Mesoporous Mater 86 (2005) 134–144.
[21] B. Yang, K. Edler, C. Guo, H. Liu, Microporous Mesoporous Mater 131 (2010) 21–27.
[22] M.H. Huang, B.S. Dunn, J.I. Zink, J. Am. Chem. Soc. 122 (2000) 3739–3745.
[23] M.R. Vicelli, C.M. Awano, D.A. Donatti, A. Ibañez Ruiz, F.S. de Vicente, A.P. Perissinotto, D.R. Vollet, Microporous Mesoporous Mater 153 (2012) 204–209.
[24] A.P. Perissinotto, C.M. Awano, D.A. Donatti, F.S. de Vicente, D.R. Vollet, Langmuir 31 (2015) 562–568.
[25] T. Freltoft, J.K. Kjems, S.K. Sinha, Phys. Rev. B 33 (1986) 269–275.
[26] J. Teixeira, J. Appl. Crystallogr. 21 (1988) 781–785.
[27] P. Debye, H.R. Anderson, H. Brumberger, J. Appl. Phys. 28 (1957) 679–683.
[28] A.F. Craievich, Small-angle X-ray scattering by nanostructured materials, in: S. Sakka, R. Almeida (Eds.), Handbook of Sol-gel Science and Technology, v.2, Kluwer, Norwell, 2005, pp. 161–189.
[29] D. Avnir, O. Biham, D. Lidar, O. Malcai, Science 279 (1998) 39–40.
[30] J.T. Koberstein, B. Morra, R.S. Stein, J. Appl. Crystallogr. 13 (1980) 34–45.
[31] G.W. Scherer, J. Non Cryst. Solids 225 (1998) 192–199.
[32] G.W. Scherer, S. Calas, R. Sempéré, J. Colloid Interface Sci. 202 (1998) 411–416.
[33] D.W. Schaefer, J.E. Martin, P. Wiltzius, D.S. Cannell, Phys. Rev. Lett. 52 (1984) 2371–2374.
[34] J. Cai, N. Lu, C.M. Sorensen, J. Colloid Interface Sci. 171 (1995) 470–473.
[35] M. Kalliat, C.Y. Kwak, P.W. Schmidt, Am. Chem. Soc. Symp. Ser. 169 (1981) 3–22.
[36] R. Vacher, T. Woignier, J. Pelous, E. Courtens, Phys. Rev. B 37 (1988) 6500–6503.